Distributional Vision-Language Alignment by Cauchy-Schwarz Divergence

Wenzhe Yin *1 Zehao Xiao *1 Pan Zhou 2 Shujian Yu 34 Jiayi Shen 1 Jan-Jakob Sonke 5 Efstratios Gavves 1

Abstract

Multimodal alignment is crucial for various downstream tasks such as cross-modal generation and retrieval. Previous multimodal approaches like CLIP maximize the mutual information mainly by aligning pairwise samples across modalities while overlooking the distributional differences, leading to suboptimal alignment with modality gaps. In this paper, to overcome the limitation, we propose CS-Aligner, a novel and straightforward framework that performs distributional vision-language alignment by integrating Cauchy-Schwarz (CS) divergence with mutual information. In the proposed framework, we find that the CS divergence and mutual information serve complementary roles in multimodal alignment, capturing both the global distribution information of each modality and the pairwise semantic relationships, yielding tighter and more precise alignment. Moreover, CS-Aligher enables incorporating additional information from unpaired data and tokenlevel representations, enhancing flexible and finegrained alignment in practice. Experiments on text-to-image generation and cross-modality retrieval tasks demonstrate the effectiveness of our method on vision-language alignment.

1. Introduction

Modality alignment is a cornerstone of multimodal representation learning, enabling success across diverse applications such as image-text retrieval (Huang et al., 2024; Koukounas et al., 2024), text-to-image (T2I) generation (Ramesh et al., 2022; Razzhigaev et al., 2023), and multimodal chatbots (Zhu et al., 2023). As a pioneering work in this field, CLIP (Radford et al., 2021) leverages contrastive loss to maximize the mutual information between paired text and image representations, effectively capturing pairwise and se-

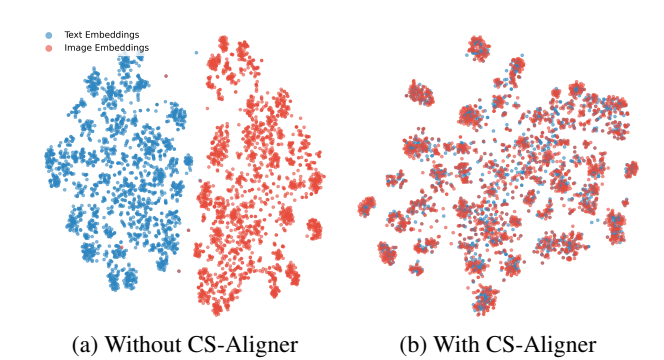


Figure 1: TSNE visualizations of CLIP text and image features without (a) and with (b) CS-Aligner. The original CLIP feature distributions reveal a clear domain gap (a). Adapting the model with our CS-Aligner effectively eliminates the modality gap, leading to tighter alignment.

mantic relationships. Its versatility has made it a foundation for many multimodal tasks.

Although widely adopted, CLIP suffers from a persistent modality gap between text and image representations in its latent space. As shown in Fig. 1a, text and image embeddings often fail to align precisely and may remain separated from each other. This modality gap has been observed and explored in prior studies (Zhou et al., 2023; Liang et al., 2022; Shi et al., 2023), which attribute the issue to factors such as cone effects (Liang et al., 2022) or suboptimal latent space structures (Shi et al., 2023). Intriguingly, Liang et al. (2022) observed a phenomenon that CLIP's contrastive learning objective may inadvertently exacerbate this gap, implying mutual information alone is insufficient for aligning text and image representation distributions.

Several strategies have been proposed to address the modality gap, such as projection modules with cosine similarity (Zhou et al., 2023; Gao et al., 2024; Huang et al., 2024) and geodesic multimodal mixup (Oh et al., 2024). UnCLIP-based models like DALL-E 2 (Ramesh et al., 2022) and Kandinsky (Razzhigaev et al., 2023) employ text-to-image prior modules (e.g., diffusion models) to map text embeddings to image feature space. A more recent alternative Eclipse (Patel et al., 2024) uses ℓ_2 loss to train a prior adapter. These works aim to transform representations across modalities for alignment. However, they remain exploring alignment sample-wisely and heavily rely on pairwise data. Although sample-wise alignment effectively cap-

^{*}Equal contribution ¹University of Amsterdam ²Singapore Management University ³Vrije Universiteit Amsterdam ⁴The Arctic University of Norway ⁵The Netherlands Cancer Institute. Correspondence to: Pan Zhou <panzhou@smu.edu.sg>.

tures semantic information, it falls short in aligning entire data distributions. Similar to the InfoNCE in CLIP, the methods struggle to match the representation spaces across modalities, ultimately limiting the overall alignment. Moreover, the reliance on carefully curated text-image pairs limits scalability and applicability to real-world scenarios with unpaired and noisy datasets (Lin et al., 2014; Li et al., 2023).

To address these challenges, we propose CS-Aligner, a novel distributional approach that incoporates Cauchy-Schwarz (CS) divergence (Principe et al., 2000b) for modality alignment. As a symmetric measure, CS divergence robustly and efficiently estimates the distance between any representation distributions without parametric distributional assumptions, making it highly suitable for multimodal distribution alignment. Furthermore, we also analyze the complementary roles of CS divergence and mutual information in multimodal alignment and propose integrating these two metrics within CS-Aligner. This enables CS-Aligner to align vision and language representations in both distributional and sample-wise levels, considering both the global modality and local semantic information, leading to more comprehensive and tighter alignment as shown in Fig. 1b.

Moreover, based on the distributional approach, CS-Aligner enables alignment with additional unpaired data, such as (a) single images with multiple captions or (b) entirely unpaired vision-language data, introducing more distributional information from richer, unstructured multimodal data for alignment robustness and flexibility in real-world scenarios. Beyond the unpaired alignment, we also introduce a novel token-level alignment scheme for vision-language models, which integrates more detailed information in diverse tokens to enhance multimodal alignment. Extensive experiments on downstream tasks, including T2I generation and imagetext retrieval, demonstrate the effectiveness of our approach.

2. Related work

Vision-language alignment and applications. CLIP (Radford et al., 2021) serves as a foundational model for visionlanguage alignment in multimodal tasks. Several works have enhanced CLIP through techniques such as momentum distillation (Li et al., 2021) and noisy text supervision (Jia et al., 2021). Despite its success, CLIP suffers from a persistent modality gap between text and image representations. Prior studies (Zhou et al., 2023; Liang et al., 2022; Shi et al., 2023) attribute this gap to factors such as cone effects (Liang et al., 2022) and suboptimal latent space structures (Shi et al., 2023). To address this, various strategies have been proposed, including projection adapters (Zhou et al., 2023; Gao et al., 2024; Huang et al., 2024), geodesic multimodal mixup (Oh et al., 2024), and parameter-efficient fine-tuning (Zanella & Ben Ayed, 2024). Recent works also improve CLIP by large language models (LLMs) (Jang

et al., 2024; Koukounas et al., 2024; Huang et al., 2024) for downstream tasks such as **image-text retrieval**.

In addition to image-text retrieval, **text-to-image (T2I) generation** is another application that reflects the vision-language alignment capability. T2I has advanced significantly over the past decades, driven by both diffusion-based (Ramesh et al., 2021; Rombach et al., 2022; Saharia et al., 2022; Nichol et al., 2021) and GAN-based models (Zhang et al., 2017; Tao et al., 2023). Among diffusion-based methods, the unCLIP framework (Ramesh et al., 2021; 2022) employs a two-stage architecture with a CLIP-guided diffusion prior and a decoder (e.g., DALL-E-2 (Ramesh et al., 2022) or Karlo (Donghoon et al., 2022)). Its prior module g_{ϕ} maps text representations ${\bf y}$ to image ones ${\bf x}$ by a diffusion model. Recently, Eclipse (Patel et al., 2024) employs an ℓ_2 loss to simplify the prior loss by eliminating diffusion time and intruding a noise ϵ term:

$$\mathcal{L}_{\text{prior}} = \mathbb{E}_{\epsilon \sim \mathcal{N}(0,I)} \left[\| \mathbf{x} - g_{\phi}(\epsilon, \mathbf{y}) \|_{2}^{2} \right]. \tag{1}$$

However, these methods still rely on pairwise loss (e.g., ℓ_2). In contrast, our approach introduces distributional alignment for a more holistic modality alignment.

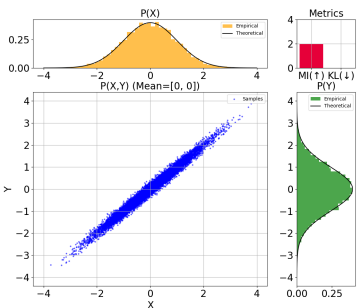
Cauchy-Schwarz divergence. The Cauchy-Schwarz (CS) divergence (Principe et al., 2000a;b) is derived from the Cauchy-Schwarz inequality for square-integrable functions. It serves as a symmetric distribution distance metric with notable properties, such as the ability to measure conditional distributions (Yu et al., 2023) and the closed-form expression for mixtures of Gaussians (Kampa et al., 2011). CS divergence has been successfully applied across various domains, including deep clustering (Trosten et al., 2021), disentangled representation learning (Tran et al., 2022), and deep regression (Yu et al., 2024). Moreover, due to its advantage of estimating discrepancy between conditional distributions, it has demonstrated success in the domain adaption area (Yin et al., 2024) and time series clustering (Yu et al., 2023). However, the utility of CS divergence in foundation models remains unclear and unexplored.

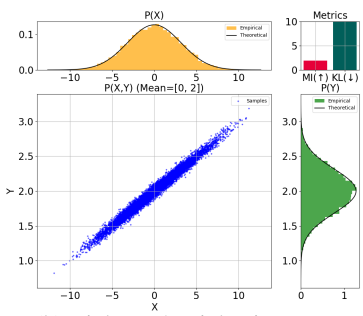
3. Methodology

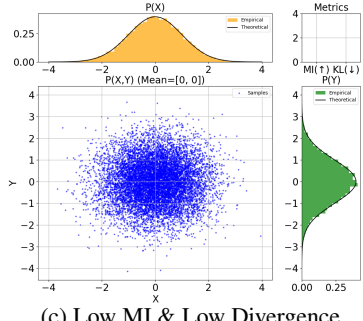
In this section, we first review the mutual information used in previous multimodal methods and analyze its limitations for alignment. Then we introduce the novel CS-Aligner framework for distributional multimodal alignment and detail the estimations of its terms. After that, we extend the method by incorporating additional distribution information. Finally, we provide parameter-efficient implementations.

3.1. Mutual Information is insufficient for alignment

Previous multimodal methods like CLIP (Radford et al., 2021) learn text and image representations in a shared space







(a) High MI & Low Divergence.

(b) High MI & High Divergence.

(c) Low MI & Low Divergence.

Figure 2: **Toy examples: mutual information and distribution divergence between two data distributions.** Distributions with the same high mutual information value can exhibit either small (a) or large (b) distributional distances, demonstrating that mutual information alone is insufficient for multimodal alignment. In addition, distribution divergence measures the closeness between distributions but does not guarantee that the underlying random variables are statistically correlated (c).

by maximizing lower bounds (e.g., InfoNCE (Oord et al., 2018)) of mutual information between modalities:

$$I(\mathbf{x}; \mathbf{y}) = \int \int p(\mathbf{x}, \mathbf{y}) \log \frac{p(\mathbf{x}, \mathbf{y})}{p(\mathbf{x})p(\mathbf{y})} d\mathbf{x} d\mathbf{y}, \quad (2)$$

where $p(\mathbf{x})$ and $p(\mathbf{y})$ are the distributions of image and text features. $p(\mathbf{x}, \mathbf{y})$ denotes the joint probability. This objective is optimized via the InfoNCE bound (Oord et al., 2018), which approximates $I(\mathbf{x}; \mathbf{y})$ using paired data samples $\{(\mathbf{x}_i, \mathbf{y}_i)\}_{i=1}^N$. We denote image-text pairs as $\{(\mathbf{x}_i, \mathbf{y}_i)\}_{i=1}^N$. The multimodal InfoNCE loss combines symmetric image-text and text-image alignment terms:

$$\mathcal{L}_{\text{InfoNCE}} = \frac{1}{2} \left(\mathcal{L}_{\text{I2T}} + \mathcal{L}_{\text{T2I}} \right),$$

$$\mathcal{L}_{\text{I2T}} = -\frac{1}{N} \sum_{i=1}^{N} \log \frac{\exp\left(\text{sim}(\mathbf{x}_{i}, \mathbf{y}_{i})/\tau\right)}{\sum_{j=1}^{N} \exp\left(\text{sim}(\mathbf{x}_{i}, \mathbf{y}_{j})/\tau\right)}, \quad (3)$$

$$\mathcal{L}_{\text{T2I}} = -\frac{1}{N} \sum_{i=1}^{N} \log \frac{\exp\left(\text{sim}(\mathbf{y}_{i}, \mathbf{x}_{i})/\tau\right)}{\sum_{j=1}^{N} \exp\left(\text{sim}(\mathbf{y}_{i}, \mathbf{x}_{j})/\tau\right)},$$

where $sim(\cdot, \cdot)$ denotes cosine similarity. τ is temperature. Critically, this formulation requires paired data $\{(x_i, y_i)\}$.

Although widely adopted, mutual information alone is insufficient for effective modality alignment (Liang et al., 2022). The reason is that mutual information quantifies the statistical dependence between two random variables (Cover, 1999), ensuring that the distribution $p(\mathbf{x})$ is related to $p(\mathbf{y})$. However, it does not guarantee that the distributions $p(\mathbf{x})$ and $p(\mathbf{y})$ are statistically similar or close to each other. In other words, two distributions can differ significantly or be far apart, yet exhibit strong dependence. We illustrate this issue with the following toy example.

Example 3.1. Consider two Gaussian distributions, $p(\mathbf{x}) \sim \mathcal{N}(\mu_{\mathbf{x}}, \sigma_{\mathbf{x}}^2)$ and $p(\mathbf{y}) \sim \mathcal{N}(\mu_{\mathbf{y}}, \sigma_{\mathbf{y}}^2)$, with a joint distribution $p(\mathbf{x}, \mathbf{y}) \sim \mathcal{N}\left(\begin{pmatrix} \mu_{\mathbf{x}} \\ \mu_{\mathbf{y}} \end{pmatrix}, \begin{pmatrix} \sigma_{\mathbf{x}}^2 & \rho \sigma_{\mathbf{x}} \sigma_{\mathbf{y}} \\ \rho \sigma_{\mathbf{x}} \sigma_{\mathbf{y}} & \sigma_{\mathbf{y}}^2 \end{pmatrix}\right)$. Here, $\mu_{\mathbf{x}}$ and $\mu_{\mathbf{y}}$ are the means of \mathbf{x} and \mathbf{y} , $\sigma_{\mathbf{x}}^2$ and $\sigma_{\mathbf{y}}^2$ are their

variances, and ρ is the correlation coefficient and controls their linear dependency. When $\rho=0.99$, the two modalities are highly dependent, with high mutual information (I=1.959); see Fig. 2a and 2b). When $\rho=0$, the modalities are independent, resulting in zero mutual information (Fig. 2c). Interestingly, two distributions with the same mutual information value can either exhibit minimal statistical distance and nearly identical shapes, including similar locations, widths, and higher-order moments, as shown in Fig. 2a, or have completely different shapes with distinct means $(0 \text{ for } p(\mathbf{x}) \text{ and } 2 \text{ for } p(\mathbf{y}))$ and variances $(100 \text{ for } p(\mathbf{x}) \text{ and } 0.01 \text{ for } p(\mathbf{y}))$, as illustrated in Fig. 2b. Quantitatively, the former case shows a minimal KL divergence of 0, while the latter exhibits a KL divergence of nearly 5, 194. See details in Appendix A.

Example 3.1 shows that despite strong dependence and high mutual information, the representation distributions of two modalities can remain misaligned and be far from each other. This issue is also observed in the CLIP model pretrained with InfoNCE, where the vision and language representations exhibit a noticeable distributional gap, as shown in Fig. 1a. This gap results in inconsistently aligned multimodal features, hindering the clear representation of shared semantics and disrupting effective mapping between modalities. Ultimately, this misalignment degrades performance in downstream tasks, including cross-modality generation.

Notably, although directly minimizing the divergence between distributions may reduce the distributional gap, it risks creating independent multimodal distributions without common semantic information (Fig. 2c). Therefore, maximizing mutual information and minimizing divergence complement each other to achieve effective multimodal representation alignment.

3.2. Distributional multimodal alignment

To overcome the limitations of mutual information term alone, we propose a distributional alignment framework. Specifically, we introduce a distribution divergence minimization regularization into the optimization of multimodal alignment, defining the overall problem as maximizing mutual information while ensuring a small divergence between multimodal distributions:

$$\max I(\mathbf{x}; \mathbf{y}), \text{ s.t. } D(p(\mathbf{x}), p(\mathbf{y})) \le \epsilon,$$
 (4)

where $\epsilon > 0$ is a small constant representing the permissible divergence threshold. To address this constrained optimization, we introduce a Lagrangian multiplier $\lambda \geq 0$, reformulating it into an unconstrained problem:

$$\min -I(\mathbf{x}; \mathbf{y}) + \lambda D(p(\mathbf{x}), p(\mathbf{y})). \tag{5}$$

This formulation optimizes for high mutual information between paired data (\mathbf{x}, \mathbf{y}) while reducing the divergence between the distributions $p(\mathbf{x})$ and $p(\mathbf{y})$.

Unlike parametric distributions, distributions of different real-world modalities exhibit unpredictable variability and inconsistent overlaps, meaning that $p(\mathbf{x})$ and $p(\mathbf{y})$ may follow arbitrary distributions with a small intersection.

Therefore, it is crucial to overcome these challenges to measure and optimize multimodal distribution divergence robustly. Below, we outline several key properties that an effective metric should satisfy for multimodal alignment.

Remark 3.2. Key properties for distribution align metrics:

- Symmetry: Both distributions are treated equally, ensuring consistent and unbiased multimodal alignment, formulated by $D(p(\mathbf{x}), p(\mathbf{y})) = D(p(\mathbf{y}), p(\mathbf{x}))$.
- Differentiable and Efficient Estimation: Enable differentiable estimation without distribution assumptions to facilitate optimization, formulated as $\partial D(p(\mathbf{x};\theta),p(\mathbf{y};\phi)) \neq \emptyset, \forall p(\mathbf{x}),p(\mathbf{y})$. Achieve the estimation non-parametrically or efficiently.
- Robustness to Small Distribution Overlap: Provide reliable measurements even when distributions have minimal overlap of supports, which may often occur in multimodal scenarios. The property is formulated as $0 \le D(p(\mathbf{x}), p(\mathbf{y})) \le \infty$ when $0 < \mu(\operatorname{supp}(p(\mathbf{x})) \cap \operatorname{supp}(p(\mathbf{y}))) < \epsilon$. $\mu(\operatorname{supp}(p(\mathbf{x})) \cap \operatorname{supp}(p(\mathbf{y})))$ denotes the overlap of $p(\mathbf{x})$ and $p(\mathbf{y})$. ϵ is a small value.

These properties enable the divergence term in (5) to align arbitrary distributions with small support overlap, which is well-suited for large-scale multimodal applications involving deep learning.

While KL divergence and Wasserstein distance are widely used, they fail to meet these requirements. KL divergence is asymmetric, inefficient for non-Gaussian data, and unreliable for distributions with small overlap (Yu et al., 2024). Similarly, Wasserstein distance is inefficient to estimate, requiring additional learnable module (Arjovsky et al., 2017)

or Sinkhorn iterations (Cuturi, 2013). As a result, these metrics are suboptimal for large-scale multimodal alignment tasks (details in Appendix B).

To satisfy these properties, we introduce CS divergence (Principe et al., 2000a;b), a symmetric and robust metric to quantify the distance between two probability density functions:

$$D_{CS}(p(\mathbf{x}); p(\mathbf{y})) = -\log\left(\frac{(\int p(\mathbf{x})p(\mathbf{y})d\mathbf{x}d\mathbf{y})^2}{\int p(\mathbf{x})^2d\mathbf{x}\int p(\mathbf{y})^2d\mathbf{y}}\right). (6)$$

The CS divergence satisfies all the desired properties. It is a symmetric distance metric between any two probability density functions $p(\mathbf{x})$ and $p(\mathbf{y})$, satisfying $0 \le D_{\text{CS}} < \infty$, with the minimum achieved if and only if $p(\mathbf{x}) = p(\mathbf{y})$. Furthermore, CS divergence can be estimated non-parametrically using a kernel density estimator (KDE) (Parzen, 1962), eliminating the need for explicit parametric assumptions about the underlying distributions. It also offers an elegant closed-form expression for mixtures of Gaussians (MoG) (Kampa et al., 2011) and infinite MoG. This provides significant flexibility in measuring distributional distance.

By incorporating the CS divergence into Eq. (5), we propose *CS-Aligner*, with the objective function:

$$\min -I(\mathbf{x}; \mathbf{y}) + \lambda D_{CS}(p(\mathbf{x}), p(\mathbf{y})). \tag{7}$$

This formulation ensures both semantic and distributional alignment, enabling robust and efficient multimodal learning across diverse real-world tasks.

3.3. CS-Aligner

We use CS-Aligner to align the pretrained multimodal models, as illustrated in Fig. 3. To enable the alignment, we detail the estimation methods for both CS divergence and mutual information in Eq. (7), providing the complete objective of CS-Aligner.

CS divergence estimation. We use KDE to estimate $D_{\text{CS}}(p(\mathbf{x}); p(\mathbf{y}))$ nonparametrically. Given *i.i.d.* samples $\{\mathbf{x}_i\}_{i=1}^M \sim p(\mathbf{x})$ and $\{\mathbf{y}_i\}_{i=1}^N \sim p(\mathbf{y})$, the empirical CS divergence estimator is given by (Jenssen et al., 2006):

$$\widehat{D}_{\text{CS}}(p(\mathbf{x}); p(\mathbf{y})) = \log \left(\frac{1}{M^2} \sum_{i,j=1}^{M} \kappa(\mathbf{x}_i, \mathbf{x}_j) \right) +$$

$$\log\left(\frac{1}{N^2}\sum_{i,j=1}^{N}\kappa(\mathbf{y}_i,\mathbf{y}_j)\right) - 2\log\left(\frac{1}{MN}\sum_{i=1}^{M}\sum_{j=1}^{N}\kappa(\mathbf{x}_i,\mathbf{y}_j)\right).$$
(8)

where κ is a kernel function such as Gaussian $\kappa_{\sigma}(\mathbf{x}, \mathbf{y}) = \exp(-\|\mathbf{x} - \mathbf{y}\|_2^2/2\sigma^2)$. This estimator is symmetric, differentiable, and computationally efficient, making it suitable for multimodal alignment. Moreover, the third term

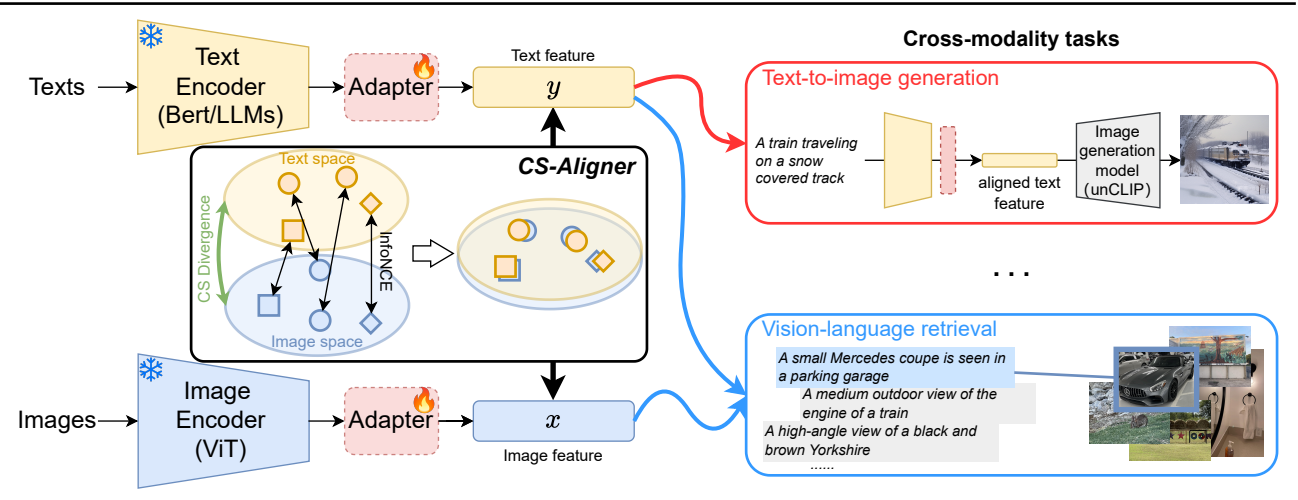


Figure 3: **Illustration of CS-Aligner.** We achieve vision-language alignment by freezing the pretrained text and image encoders and applying parameter-efficient fine-tuning methods (e.g., adapter) with our CS-Aligner. CS-Aligner optimizes the adapters using the aggregated CS divergence and InfoNCE, as formulated in Eq. (5). Once aligned, the adapters are utilized for various cross-modality tasks: the aligned text adapter facilitates text-to-image generation without additional modifications, while the aligned multimodal adapters are used for vision-language retrieval.

in Eq. (8) ensures that $\widehat{D}_{\text{CS}}(p(\mathbf{x});p(\mathbf{y})) \to \infty$ only when $\kappa(\mathbf{x},\mathbf{y}) \to 0$ (i.e., when the distributions do not overlap). However, as long as there is nonzero overlap between the distributions, the estimator remains well-defined and valid. **Remark** 3.3. Connection to the prior loss (ℓ_2 loss) (Patel et al., 2024). Consider the third term in Eq. (8), which involves $\kappa(\mathbf{x}_i,\mathbf{y}_j)$ defined by the Gaussian kernel $\kappa_{\sigma}(\mathbf{x},\mathbf{y}) = \exp(-\|\mathbf{x}-\mathbf{y}\|_2^2/2\sigma^2)$. A second-order Taylor expansion yields

$$\kappa(\mathbf{x}_i, \mathbf{y}_j) = \exp\left(-\frac{(\mathbf{x}_i - \mathbf{y}_j)^2}{2\sigma^2}\right) \approx 1 - \frac{(\mathbf{x}_i - \mathbf{y}_j)^2}{2\sigma^2}.$$
 (9)

When i=j (i.e., diagonal of $\kappa(\mathbf{x},\mathbf{y})$), this approximation reduces to a weighted ℓ_2 loss by $1/2\sigma^2$, analogous to the Eq. 1. Consequently, the ℓ_2 loss emerges as a special case of our divergence, focusing solely on paired sample reconstruction and omitting broader distribution alignment, including off-diagonal (cross-sample) contributions.

Mutual information estimation. The mutual information and the CS divergence serve complementary roles for alignment: mutual information captures semantic relationships by focusing on pairwise samples, while CS divergence aligns modalities at the distributional level (overall data distribution), leveraging global information.

Inspired by CLIP-based methods (Radford et al., 2021), we estimate the mutual information term $I(\mathbf{x}, \mathbf{y})$ in Eq. (5)using its lower bound, optimized via InfoNCE (Eq. (3)). We specifically choose InfoNCE not only for the optimization efficiency but also for its compatibility with CS divergence in the cosine similarity space.

Remark 3.4. The connection between CS divergence and InfoNCE becomes evident when analyzing both terms from

a cosine similarity perspective. For a characteristic kernel $\kappa(\mathbf{x},\mathbf{y}) = \langle \phi(\mathbf{x}),\phi(\mathbf{y})\rangle_{\mathcal{H}}$, where ϕ maps samples to a Reproducing Kernel Hilbert Space (RKHS) \mathcal{H} , the mean embeddings are: $\mu_x = \frac{1}{m}\sum_{i=1}^m \phi(\mathbf{x}_i)$ and $\mu_y = \frac{1}{n}\sum_{i=1}^n \phi(\mathbf{y}_i)$, The CS divergence can then be expressed as:

$$\hat{D}_{CS}(p(\mathbf{x}); p(\mathbf{y})) = -2\log\left(\frac{\langle \boldsymbol{\mu}_x, \boldsymbol{\mu}_y \rangle_{\mathcal{H}}}{\|\boldsymbol{\mu}_x\|_{\mathcal{H}} \|\boldsymbol{\mu}_y\|_{\mathcal{H}}}\right)$$

$$= -2\log\sin(\boldsymbol{\mu}_x, \boldsymbol{\mu}_y),$$
(10)

which evaluates the cosine similarity between distributions. Similarly, InfoNCE evaluates cosine similarity between paired samples (Eq. 3). This dual-level similarity assessment underscores the synergy between CS divergence and mutual information, offering a unified and robust framework for multimodal alignment.

Final objective function. With the exact estimation of the CS divergence in Eq. (8) and InfoNCE in Eq. (3), the final objective function of our method is formulated as:

$$\mathcal{L}_{\text{CS-Aligner}} = \widehat{D}_{\text{CS}}(p(\mathbf{x}); p(\mathbf{y})) + \lambda \mathcal{L}_{\text{InfoNCE}}.$$
 (11)

3.4. Extended alignment with unpaired data

Benefits from the distributional alignment, we further propose some novel extensions of CS-Aligner, which leverage additional information in unpaired data. While mutual information estimation requires pairwise data, the CS divergence estimator (Eq. (8)) can operate seamlessly on unpaired data without introducing additional computation. This unique capability enables CS-Aligner to extend beyond traditional pairwise multimodal alignment by incorporating additional distributional information from unpaired data or tokens. We

introduce two novel directions for this extended alignment: unpaired data alignment and token alignment.

Unpaired vision-language alignment. Our method leverages two forms of unpaired alignments: (1) images with multiple captions, and (2) independently sampled unpaired images and texts. The unpaired alignments are achieved using Eq. (8), where $\{x_i\}_{i=1}^M$ and $\{y_j\}_{j=1}^N$ can be independent with $M \neq N$. In both scenarios, our method leverages more uncurated unpaired data for distributional multimodal alignment, providing greater flexibility and robustness.

Vision-language token alignment. We also propose a novel intra-sample distribution alignment approach between vision and language tokens. Unlike CLIP-based models (Radford et al., 2021), which align only the "CLS" tokens of vision and text representations, the method considers all vision and text tokens for a more fine-grained alignment. Specifically, each vision feature $\mathbf{x}_i \in \mathbb{R}^{V \times D}$ is modeled as a token distribution $p(\mathbf{x}_i)$ containing V vision tokens, while each text feature $\mathbf{y}_i \in \mathbb{R}^{L \times D}$ is represented as a token distribution $p(\mathbf{y}_i)$ consisting of L text tokens. D denotes the feature dimension. We compute the CS divergence between the vision and text token distributions. The internal token-wise alignment loss $\mathcal{L}_{\text{token}}$ is formulated as:

$$\mathcal{L}_{\text{token}} = \frac{1}{B} \sum_{i=1}^{B} \widehat{D}_{\text{CS}}(p(\mathbf{x}_i); p(\mathbf{y}_i)), \tag{12}$$

where B is the batch size. In general, $V \neq L$, and vision and language tokens do not have a direct pairing, making InfoNCE inapplicable for estimation. Through our distributional alignment, Eq. (12) enables comprehensive alignment across all tokens, capturing more details and potentially enhancing fine-grained alignment.

3.5. Parameter-efficient multimodal alignment

We demonstrate the effectiveness of our CS-Aligner by performing vision-language alignment in a parameter-efficient manner using pretrained vision and language models, such as CLIP and large language models (LLMs) (Dubey et al., 2024). To adapt these pretrained models, we employ two widely used frameworks: adapter (Gao et al., 2024) and LoRA (Low-Rank Adaptation) (Hu et al., 2021).

Adapter alignment. We add a lightweight transformer (Vaswani, 2017) on top of the pretrained model as an adapter. The adapter projects text embeddings or image embeddings into a shared representation space and distribution.

LoRA alignment. We also explore LoRA to insert trainable low-rank matrices into the pretrained weights of the text encoder. It enables fine-grained adjustments to the representations, aligning them with the other modality distribution.

The adapter and LoRA enable efficient alignment of the

multimodal large-scale pretrained models, without requiring extensive computational resources.

4. Experiments

We evaluate our method on two tasks to illustrate its vision-language alignment ability: text-to-image (T2I) generation in Section 4.1 and image-text retrieval in Section 4.2.

4.1. Text to image generation

Datasets. Following a previous T2I approach (Patel et al., 2024), we train our method on four datasets: **MSCOCO** (Lin et al., 2014), **CC3M** (Sharma et al., 2018), **CC12M** (Changpinyo et al., 2021), and **LAION-HighResolution-5M** (Schuhmann et al., 2022). MSCOCO contains 80K images paired with multiple captions. CC3M and CC12M include about 2.5M and 10M image-text pairs, respectively. LAION-HighResolution comprises 175M high-resolution pairs, from which we select 5M for training. We evaluate the aligned model on the MSCOCO 30K validation set.

Experimental setup. We build our method based on unCLIP-style approaches (e.g., DALL-E-2 (Ramesh et al., 2022), Karlo (Donghoon et al., 2022), Kandinsky (Razzhigaev et al., 2023)). These methods typically train a diffusion prior module on large-scale datasets (more than hundreds of millions data) to map text representations into the image representation space. The diffused text representations are fed into a separate decoder for image generation.

Differently, CS-Aligner trains an adapter to align text representations to image feature space on small-scale datasets, e.g., MSCOCO (0.08M), CC3M (3M), and CC12M (12M), and LAION-HighRes subset (5M). After alignment, we directly process the aligned text features using the pretrained decoder of the large-scale methods (e.g., Karlo and Kandinsky) to generate images, without additional prior modules or multiple diffusion steps. We evaluate generation quality with the FID score (Heusel et al., 2017), which measures how closely generated images match the real image distribution. This metric is particularly well-suited for evaluating modality alignment, as it directly reflects the distribution distance. Additional details can be found in Appendix C.

Baselines. Our baselines consists of both large-scale methods Karlo (Donghoon et al., 2022), Kandinsky (Razzhigaev et al., 2023) and recent small-scale alignment method Eclipse (Patel et al., 2024). Eclipse streamlines the prior module in Karlo and Kandinsky by employing an L_2 loss for T2I. For a fair comparison, we adopt the same Transformer adapter as Eclipse and only align the "CLS" tokens, highlighting the advantages of our distributional alignment.

Comparisons. We compare our method with both the large-scale diffusion-based methods and the small-scale alignment

Table 1: **Comparisons with T2I methods.** Our method outperforms both large-scale diffusion-based methods (Karlo, Kandinsky) and the recent small-scale method Eclipse.

Methods	Datasize (M)	FID
Large-scale methods		
DALL-E2	250	10.65
Kandinsky	177	20.48
Karlo	115	20.64
Small-scale alignment		
Eclipse + Kandinsky decoder	$0.08_{(COCO)}$	16.53
Ours + Kandinsky decoder	$0.08_{(COCO)}$	12.62
Eclipse + Karlo decoder	$0.08_{(COCO)}$	23.67
Ours + Karlo decoder	$0.08_{(COCO)}$	11.27

Table 2: **Comparisons with Eclipse on various training data.** Our method consistently performs better.

Method	CC3M	CC12M	LAION-HighRes 5M
Eclipse	26.73	26.98	19.16
Ours	22.88	22.72	14.79

methods. The results are provided in Table 1. By aligning text representations to image representations on the small MSCOCO data, our method achieves superior T2I generation than the large-scale methods Karlo and Kandinsky, without any diffusion steps. CS-Aligner also outperforms Eclipse by an obvious margin using either Karlo or Kandinsky decoders. The results demonstrate the effective vision-language alignment capability of our method. Moreover, we compare CS-Aligner with Eclipse across different training datasets. As shown in Table 2, our method performs better across diverse training data (CC3M, CC12M, and LAION-HighRes-5M), underscoring the importance of the modality distribution information for robust alignment.

Qualitative Visualization. To further evaluate our method, we present qualitative visualizations of generated images using the Karlo decoder. As shown in Fig. 4, our aligned text representations result in more realistic images with stronger semantic consistency with the input sentence, highlighting the effectiveness of CS-Aligner in enhancing alignment.

CS-Aligner with different adaptation approaches. To demonstrate the robustness of our method across different models, we perform alignments for T2I using both adapter and LoRA. Specifically, we apply LoRA with a low-rank dimension of 8 to every transformer layer in the CLIP text encoder. As shown in Table 3, based on either Karlo or Kandinsky, CS-Aligner with LoRA introduces fewer parameters, while still achieving comparable results compared with the adapter-based one, demonstrating the effectiveness and adaptability of CS-Aligner across different models.

CS-Aligner with multiple captions. It is common in real-

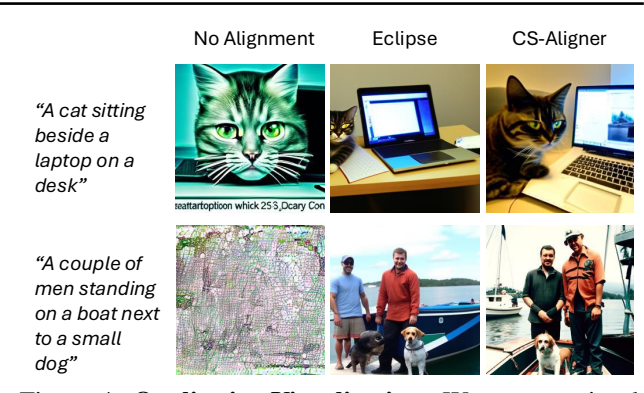


Figure 4: **Qualitative Visualization.** We present visualizations for no alignment (left), Eclipse (middle), and CS-Aligner (right). CS-Aligner achieves more realistic generations with stronger semantic consistency.

Table 3: **CS-Aligner with different adaptation approaches.** Our method achieves good alignment using both adapter and LoRA.

Base Model	Adaptation	#Parameters	FID
Kandinsky	Adapter	34M	12.62
	LoRA	6M	13.52
Karlo	Adapter	33M	11.27
	LoRA	1.3M	15.63

world datasets for a single image to correspond to multiple captions (e.g., 5 captions per image in MSCOCO). Due to their pairwise alignment nature, previous methods such as InfoNCE and ℓ_2 -based approaches (Radford et al., 2021; Patel et al., 2024) struggle to simultaneously leverage multiple captions. In contrast, by incorporating CS divergence, our CS-Aligner enables training for alignment with single image and multiple captions. To demonstrate the benefits of multiple captions for CS-Aligner, we conducted experiments on the MSCOCO dataset by estimating the CS divergence term \widehat{D}_{CS} in Eq. (11) using both single and multiple captions. As shown in Fig. 5a, CS-Aligner effectively leverages the information provided by multiple captions, leading to improved vision-language alignment.

CS-Aligner with additional unpaired data. Collecting and accurately annotating paired vision-language data is both challenging and costly. Enhancing alignment with additional unpaired data offers a more flexible and scalable solution for real-world applications. However, similar to the case of multiple captions, previous methods (Radford et al., 2021; Patel et al., 2024) struggle to fully utilize unpaired data due to their reliance on pairwise alignment, whereas CS-Aligner naturally incorporates the unpaired data information by CS divergence. To demonstrate this capability, we conduct experiments on the MSCOCO dataset using the Kandinsky decoder with (1) 80K paired training samples, (2) 40K paired training samples, and (3) 40K paired training samples supplemented with 80K unpaired samples, where

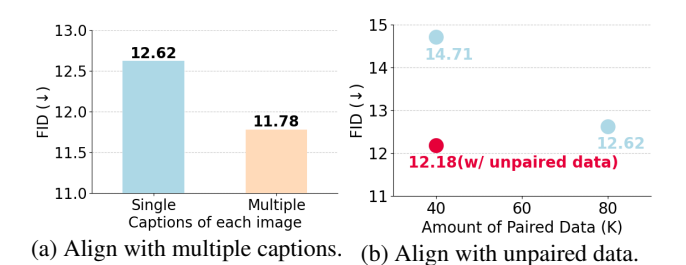


Figure 5: **CS-Aligner with additional information.** Our method benefits from the additional information from the multiple captions (a) and unpaired data (b).



Figure 6: **CS-Aligner with token alignment.** Token alignment enhance more fine-grained vision-language alignment.

the unpaired samples are used to estimate the CS divergence. As shown in Fig. 5b, the result with 40K paired training data is lower than 80K. However, introducing additional unpaired data obviously improves the performance, even surpassing the model trained with 80K paired samples. This demonstrates CS-Aligner's ability to effectively leverage the distributional information of modalities for alignment.

CS-Aligner with token alignment. Beyond the unpaired data, CS-Aligner also enables token-level alignment by treating the tokens of each sample as a distribution. We evaluated the token-level extension of CS-Aligner using the Kandinsky decoder on the MSCOCO dataset. As shown in Fig. 6, incorporating token alignment further improves performance. Moreover, qualitative results indicate that token alignment enhances fine-grained details in generated images, suggesting an improved ability to capture fine-grained relationships between modalities. Additional visualizations are provided in Fig. 8 in Appendix D.2.

4.2. Image-Text Retrieval

Experimental Setup. Effective multimodal alignment also benefits cross-model retrieval. To demonstrate the align-

Table 4: Comparisons of image-to-text (I2T) and text-to-image (T2I) retrieval. Our method outperforms the baselines on diverse datasets.

	Flickr30k		Urban-1k		DOCCI		Average	
Methods	I2T	T2I	I2T	T2I	I2T	T2I	I2T	T2I
Long-CLIP	90.0	76.2	82.5	86.1	66.5	78.6	79.7	80.3
CLIP	85.2	65.0	68.3	55.6	63.1	65.8	72.2	62.1
LLM2CLIP-3M	89.6	77.3	87.1	91.1	84.9	87.8	87.2	85.4
Ours-3M	91.8	81.0	87.6	92.2	86.6	89.1	88.7	87.4

ment ability of our method on retrieval tasks, we conduct experiments aligning LLMs (Dubey et al., 2024) text representations with CLIP vision representations on both image-to-text and text-to-image retrieval. We use the Flickr 1K test set (Young et al., 2014) for short-text retrieval, while Urban1K (Zhang et al., 2025) and DOCCI (Onoe et al., 2025) are employed for long-text retrieval. We compare CS-Aligner against pure InfoNCE-based methods, such as Long-CLIP (Zhang et al., 2025) and LLM2CLIP (Huang et al., 2024), as the baselines. To ensure a fair comparison, we adopt the setup from LLM2CLIP, aligning CLIP ViT-L/14 image representations with Llama 3 (8B) text representations. Both the vision and text representations are aligned by adapters trained on the CC3M dataset.

Comparisons. The results in Table 4 show that our method consistently and significantly outperforms the baselines across various datasets for both image-to-text (I2T) and text-to-image (T2I) retrieval. This demonstrates the effectiveness of our method for aligning the two modalities into a shared space. Moreover, the ability to align a different text encoder (LLM) with the successful alignment of an LLM-based text encoder with the CLIP image encoder highlights the flexibility and generalizability of our approach.

5. Conclusion

In this paper, we propose CS-Aligner, a novel distributional alignment framework that integrates Cauchy–Schwarz (CS) divergence with mutual information for multimodal alignment. By combining global distributional alignment with InfoNCE, CS-Aligner achieves tighter and more comprehensive alignment. By considering the modality distributional information, our method enables to leverage additional and detailed information from unpaired samples and tokens, leading to more flexible and fine-grained information for alignment. We demonstrate the effectiveness of our alignment on text-to-image generation and cross-modal retrieval.

Limitation & future work. Although our method has numerous applications, it is currently evaluated only on unCLIP-type models for generation. In the future, we will explore its integration with stable-diffusion-based models. Broader modalities (e.g., audio and video) and diverse tasks (e.g., image-to-text generation) could further strengthen alignment and broaden the applicability of CS-Aligner.

Impact Statement

This paper contributes to the advancement of Machine Learning. While our work may have various societal implications, none require specific emphasis at this stage.

References

- Arjovsky, M., Chintala, S., and Bottou, L. Wasserstein generative adversarial networks. In *International conference on machine learning*, pp. 214–223. PMLR, 2017.
- Changpinyo, S., Sharma, P., Ding, N., and Soricut, R. Conceptual 12m: Pushing web-scale image-text pre-training to recognize long-tail visual concepts. In *Proceedings of the IEEE/CVF conference on computer vision and pattern recognition*, pp. 3558–3568, 2021.
- Cover, T. M. Elements of information theory. John Wiley & Sons, 1999.
- Cuturi, M. Sinkhorn distances: Lightspeed computation of optimal transport. *Advances in neural information processing systems*, 26, 2013.
- Donghoon, L., Jiseob, K., Jisu, C., Jongmin, K., Minwoo, B., Woonhyuk, B., and Saehoon, K. Karlo-v1.0.alpha on coyo-100m and cc15m. https://github.com/kakaobrain/karlo, 2022.
- Dubey, A., Jauhri, A., Pandey, A., Kadian, A., Al-Dahle, A., Letman, A., Mathur, A., Schelten, A., Yang, A., Fan, A., et al. The llama 3 herd of models. *arXiv preprint arXiv:2407.21783*, 2024.
- Gao, P., Geng, S., Zhang, R., Ma, T., Fang, R., Zhang, Y., Li, H., and Qiao, Y. Clip-adapter: Better vision-language models with feature adapters. *International Journal of Computer Vision*, 132(2):581–595, 2024.
- Heusel, M., Ramsauer, H., Unterthiner, T., Nessler, B., and Hochreiter, S. Gans trained by a two time-scale update rule converge to a local nash equilibrium. *Advances in neural information processing systems*, 30, 2017.
- Ho, J. and Salimans, T. Classifier-free diffusion guidance. *arXiv preprint arXiv:2207.12598*, 2022.
- Ho, J., Jain, A., and Abbeel, P. Denoising diffusion probabilistic models. *Advances in neural information processing systems*, 33:6840–6851, 2020.
- Hu, E. J., Shen, Y., Wallis, P., Allen-Zhu, Z., Li, Y., Wang, S., Wang, L., and Chen, W. Lora: Low-rank adaptation of large language models. arXiv preprint arXiv:2106.09685, 2021.

- Huang, W., Wu, A., Yang, Y., Luo, X., Yang, Y., Hu, L., Dai, Q., Dai, X., Chen, D., Luo, C., et al. Llm2clip: Powerful language model unlock richer visual representation. *arXiv* preprint arXiv:2411.04997, 2024.
- Jang, Y. K., Kang, J., Lee, Y. J., and Kim, D. Mate: Meet at the embedding–connecting images with long texts. *arXiv* preprint arXiv:2407.09541, 2024.
- Jenssen, R., Principe, J. C., Erdogmus, D., and Eltoft, T. The cauchy–schwarz divergence and parzen windowing: Connections to graph theory and mercer kernels. *Journal of the Franklin Institute*, 343(6):614–629, 2006.
- Jia, C., Yang, Y., Xia, Y., Chen, Y.-T., Parekh, Z., Pham, H., Le, Q., Sung, Y.-H., Li, Z., and Duerig, T. Scaling up visual and vision-language representation learning with noisy text supervision. In *International conference on* machine learning, pp. 4904–4916. PMLR, 2021.
- Kampa, K., Hasanbelliu, E., and Principe, J. C. Closed-form cauchy-schwarz pdf divergence for mixture of gaussians. In *The 2011 International Joint Conference on Neural Networks*, pp. 2578–2585. IEEE, 2011.
- Korotin, A., Selikhanovych, D., and Burnaev, E. Neural optimal transport. *arXiv preprint arXiv:2201.12220*, 2022.
- Koukounas, A., Mastrapas, G., Günther, M., Wang, B., Martens, S., Mohr, I., Sturua, S., Akram, M. K., Martínez, J. F., Ognawala, S., et al. Jina clip: Your clip model is also your text retriever. arXiv preprint arXiv:2405.20204, 2024.
- Li, J., Selvaraju, R., Gotmare, A., Joty, S., Xiong, C., and Hoi, S. C. H. Align before fuse: Vision and language representation learning with momentum distillation. *Advances in neural information processing systems*, 34: 9694–9705, 2021.
- Li, T., Bhardwaj, S., Tian, Y., Zhang, H., Barber, J., Katabi, D., Lajoie, G., Chang, H., and Krishnan, D. Leveraging unpaired data for vision-language generative models via cycle consistency. *arXiv preprint arXiv:2310.03734*, 2023.
- Liang, V. W., Zhang, Y., Kwon, Y., Yeung, S., and Zou, J. Y. Mind the gap: Understanding the modality gap in multi-modal contrastive representation learning. *Advances in Neural Information Processing Systems*, 35: 17612–17625, 2022.
- Lin, T.-Y., Maire, M., Belongie, S., Hays, J., Perona, P., Ramanan, D., Dollár, P., and Zitnick, C. L. Microsoft coco: Common objects in context. In *Computer Vision–ECCV 2014: 13th European Conference, Zurich, Switzerland, September 6-12, 2014, Proceedings, Part V 13*, pp. 740–755. Springer, 2014.

- Nichol, A., Dhariwal, P., Ramesh, A., Shyam, P., Mishkin, P., McGrew, B., Sutskever, I., and Chen, M. Glide: Towards photorealistic image generation and editing with text-guided diffusion models. *arXiv preprint arXiv:2112.10741*, 2021.
- Oh, C., So, J., Byun, H., Lim, Y., Shin, M., Jeon, J.-J., and Song, K. Geodesic multi-modal mixup for robust fine-tuning. *Advances in Neural Information Processing Systems*, 36, 2024.
- Onoe, Y., Rane, S., Berger, Z., Bitton, Y., Cho, J., Garg, R., Ku, A., Parekh, Z., Pont-Tuset, J., Tanzer, G., et al. Docci: Descriptions of connected and contrasting images. In *European Conference on Computer Vision*, pp. 291–309. Springer, 2025.
- Oord, A. v. d., Li, Y., and Vinyals, O. Representation learning with contrastive predictive coding. *arXiv* preprint *arXiv*:1807.03748, 2018.
- Parzen, E. On estimation of a probability density function and mode. *The annals of mathematical statistics*, 33(3): 1065–1076, 1962.
- Patel, M., Kim, C., Cheng, S., Baral, C., and Yang, Y. Eclipse: A resource-efficient text-to-image prior for image generations. In *Proceedings of the IEEE/CVF Conference on Computer Vision and Pattern Recognition*, pp. 9069–9078, 2024.
- Principe, J. C., Xu, D., Fisher, J., and Haykin, S. Information theoretic learning. *Unsupervised adaptive filtering*, 1:265–319, 2000a.
- Principe, J. C., Xu, D., Zhao, Q., and Fisher, J. W. Learning from examples with information theoretic criteria. *Journal of VLSI signal processing systems for signal, image and video technology*, 26:61–77, 2000b.
- Radford, A., Kim, J. W., Hallacy, C., Ramesh, A., Goh, G., Agarwal, S., Sastry, G., Askell, A., Mishkin, P., Clark, J., et al. Learning transferable visual models from natural language supervision. In *International conference on machine learning*, pp. 8748–8763. PMLR, 2021.
- Ramesh, A., Pavlov, M., Goh, G., Gray, S., Voss, C., Radford, A., Chen, M., and Sutskever, I. Zero-shot text-to-image generation. In *International conference on machine learning*, pp. 8821–8831. Pmlr, 2021.
- Ramesh, A., Dhariwal, P., Nichol, A., Chu, C., and Chen, M. Hierarchical text-conditional image generation with clip latents. *arXiv* preprint arXiv:2204.06125, 1(2):3, 2022.
- Razzhigaev, A., Shakhmatov, A., Maltseva, A., Arkhipkin, V., Pavlov, I., Ryabov, I., Kuts, A., Panchenko, A., Kuznetsov, A., and Dimitrov, D. Kandinsky: an improved

- text-to-image synthesis with image prior and latent diffusion. *arXiv preprint arXiv:2310.03502*, 2023.
- Rombach, R., Blattmann, A., Lorenz, D., Esser, P., and Ommer, B. High-resolution image synthesis with latent diffusion models. In *Proceedings of the IEEE/CVF conference on computer vision and pattern recognition*, pp. 10684–10695, 2022.
- Saharia, C., Chan, W., Saxena, S., Li, L., Whang, J., Denton,
 E. L., Ghasemipour, K., Gontijo Lopes, R., Karagol Ayan,
 B., Salimans, T., et al. Photorealistic text-to-image diffusion models with deep language understanding. *Advances in neural information processing systems*, 35: 36479–36494, 2022.
- Schuhmann, C., Beaumont, R., Vencu, R., Gordon, C., Wightman, R., Cherti, M., Coombes, T., Katta, A., Mullis, C., Wortsman, M., et al. Laion-5b: An open large-scale dataset for training next generation image-text models. *Advances in Neural Information Processing Systems*, 35: 25278–25294, 2022.
- Sharma, P., Ding, N., Goodman, S., and Soricut, R. Conceptual captions: A cleaned, hypernymed, image alt-text dataset for automatic image captioning. In *Proceedings of the 56th Annual Meeting of the Association for Computational Linguistics (Volume 1: Long Papers)*, pp. 2556–2565, 2018.
- Shi, P., Welle, M. C., Björkman, M., and Kragic, D. Towards understanding the modality gap in clip. In *ICLR 2023 Workshop on Multimodal Representation Learning: Perks and Pitfalls*, 2023.
- Tao, M., Bao, B.-K., Tang, H., and Xu, C. Galip: Generative adversarial clips for text-to-image synthesis. In *Proceed-ings of the IEEE/CVF Conference on Computer Vision and Pattern Recognition*, pp. 14214–14223, 2023.
- Tran, L., Pantic, M., and Deisenroth, M. P. Cauchy-schwarz regularized autoencoder. *Journal of Machine Learning Research*, 23, 2022.
- Trosten, D. J., Lokse, S., Jenssen, R., and Kampffmeyer, M. Reconsidering representation alignment for multi-view clustering. In *Proceedings of the IEEE/CVF conference on computer vision and pattern recognition*, pp. 1255–1265, 2021.
- Vaswani, A. Attention is all you need. *Advances in Neural Information Processing Systems*, 2017.
- Wang, Q., Kulkarni, S. R., and Verdú, S. Divergence estimation for multidimensional densities via *k*-nearest-neighbor distances. *IEEE Transactions on Information Theory*, 55(5):2392–2405, 2009.

- Yin, W., Yu, S., Lin, Y., Liu, J., Sonke, J.-J., and Gavves, S. Domain adaptation with cauchy-schwarz divergence. In The 40th Conference on Uncertainty in Artificial Intelligence, 2024.
- Young, P., Lai, A., Hodosh, M., and Hockenmaier, J. From image descriptions to visual denotations: New similarity metrics for semantic inference over event descriptions. *Transactions of the Association for Computational Linguistics*, 2:67–78, 2014.
- Yu, S., Li, H., Løkse, S., Jenssen, R., and Príncipe, J. C. The conditional cauchy-schwarz divergence with applications to time-series data and sequential decision making. *arXiv* preprint arXiv:2301.08970, 2023.
- Yu, S., Yu, X., Løkse, S., Jenssen, R., and Principe, J. C. Cauchy-schwarz divergence information bottleneck for regression. *arXiv* preprint arXiv:2404.17951, 2024.
- Zanella, M. and Ben Ayed, I. Low-rank few-shot adaptation of vision-language models. In *Proceedings of the IEEE/CVF Conference on Computer Vision and Pattern Recognition*, pp. 1593–1603, 2024.
- Zhang, B., Zhang, P., Dong, X., Zang, Y., and Wang, J. Long-clip: Unlocking the long-text capability of clip. In European Conference on Computer Vision, pp. 310–325. Springer, 2025.
- Zhang, H., Xu, T., Li, H., Zhang, S., Wang, X., Huang, X., and Metaxas, D. N. Stackgan: Text to photo-realistic image synthesis with stacked generative adversarial networks. In *Proceedings of the IEEE international conference on computer vision*, pp. 5907–5915, 2017.
- Zheng, C., Vuong, T.-L., Cai, J., and Phung, D. Movq: Modulating quantized vectors for high-fidelity image generation. *Advances in Neural Information Processing Systems*, 35:23412–23425, 2022.
- Zhou, C., Zhong, F., and Öztireli, C. Clip-pae: projection-augmentation embedding to extract relevant features for a disentangled, interpretable and controllable text-guided face manipulation. In ACM SIGGRAPH 2023 Conference Proceedings, pp. 1–9, 2023.
- Zhu, D., Chen, J., Shen, X., Li, X., and Elhoseiny, M. Minigpt-4: Enhancing vision-language understanding with advanced large language models. *arXiv* preprint *arXiv*:2304.10592, 2023.

A. Details of the toy examples

Mutual information. For two continuous random variables x and y, the mutual information is defined as:

$$I(\mathbf{x}; \mathbf{y}) = \iint p(\mathbf{x}, \mathbf{y}) \log \left(\frac{p(\mathbf{x}, \mathbf{y})}{p(\mathbf{x}) p(\mathbf{y})} \right) d\mathbf{x} d\mathbf{y}.$$
 (13)

For a bivariate Gaussian distribution

$$p(\mathbf{x}, \mathbf{y}) \sim \mathcal{N}\left(\begin{pmatrix} \mu_{\mathbf{x}} \\ \mu_{\mathbf{y}} \end{pmatrix}, \begin{pmatrix} \sigma_{\mathbf{x}}^2 & \rho \sigma_{\mathbf{x}} \sigma_{\mathbf{y}} \\ \rho \sigma_{\mathbf{x}} \sigma_{\mathbf{y}} & \sigma_{\mathbf{y}}^2 \end{pmatrix}\right),$$

the mutual information admits the closed-form solution:

$$I(\mathbf{x}; \mathbf{y}) = -\frac{1}{2} \ln(1 - \rho^2). \tag{14}$$

In particular, for correlation $\rho = 0.99$, we have $I(\mathbf{x}, \mathbf{y}) \approx 1.959$, while for $\rho = 0$, the variables are independent and $I(\mathbf{x}, \mathbf{y}) = 0$.

Divergence. For univariate Gaussian distributions $p(\mathbf{x}) = \mathcal{N}(\mu_{\mathbf{x}}, \sigma_{\mathbf{x}}^2)$ and $p(\mathbf{y}) = \mathcal{N}(\mu_{\mathbf{y}}, \sigma_{\mathbf{y}}^2)$, the KL divergence is given by:

$$D_{\mathrm{KL}}(p(\mathbf{x}) \parallel p(\mathbf{y})) = \ln \left(\frac{\sigma_{\mathbf{y}}}{\sigma_{\mathbf{x}}}\right) + \frac{\sigma_{\mathbf{x}}^{2} + (\mu_{\mathbf{x}} - \mu_{\mathbf{y}})^{2}}{2 \sigma_{\mathbf{y}}^{2}} - \frac{1}{2}.$$
 (15)

For Fig. 2a and Fig. 2c, we set $\sigma_{\mathbf{x}} = \sigma_{\mathbf{y}} = 1$. Hence, when $\mu_{\mathbf{x}} = \mu_{\mathbf{y}} = 0$, $D_{\mathrm{KL}} \big(p(\mathbf{x}) \parallel p(\mathbf{y}) \big) = 0$.

For Fig. 2b, we use $\sigma_x = 10$ and $\sigma_y = 0.1$. When $\mu_{\mathbf{x}} = 0$ and $\mu_{\mathbf{y}} = 2$, the $D_{\mathrm{KL}}(p(\mathbf{x}) \parallel p(\mathbf{y})) = 5194.89$, which is very large.

B. Comparison bwtween CS divergence and other metrics

In the following, we analyze why CS divergence is a better choice than well-known KL divergence and Wasserstein distance.

Comparison with KL divergence. KL divergence, a widely used metric in deep learning, is defined as:

$$D_{KL}(p(\mathbf{x})||p(\mathbf{y})) = \int p(\mathbf{x}) \log \frac{p(\mathbf{x})}{p(\mathbf{y})} d\mathbf{x},$$
(16)

where $p(\mathbf{x})$ and $p(\mathbf{y})$ are the probability distributions being compared. However, KL divergence is a non-symmetric metric, making it less suitable for learning a shared representation space (bi-directional), as commonly needed in multi-modal learning.

Minimal distribution overlap requirement. Furthermore, KL divergence can diverge to infinity when the distributions $p(\mathbf{x})$ and $p(\mathbf{y})$ have minimal overlap, making it invalid. In contrast, CS divergence remains well-defined under such conditions and provides a stable estimation (Yu et al., 2024; Yin et al., 2024). This issue is particularly critical in multi-modality settings, where the distributions from different modalities may have limited overlap.

Nonparametric estimation. Additionally, when the distributions are not assumed to be Gaussian, a nonparametric estimator is required for KL divergence. A common choice, the k-NN estimator (Wang et al., 2009), is non-differentiable, which poses challenges for optimization in gradient-based learning frameworks. In contrast, the CS divergence demonstrates greater stability and differentiability when paired with KDE, making it a more robust choice.

Comparison with wasserstein distance. Wasserstein Distance is also widely used for distribution discrepancy (e.g. GAN (Arjovsky et al., 2017)). However, Wasserstein distance is be computed either by using an additional learnable module (e.g., a neural network for estimating a transport map (Korotin et al., 2022)) or by solving an optimization problem, often approximated via multiple Sinkhorn (Cuturi, 2013) iterations for computational efficiency, leading to efficiency problem in large-scale training. In contrast, CS divergence can be efficiently estimated by a nonparametric estimator.

C. Implementation details

Implementation details Our models were trained on 4 NVIDIA RTX A100 GPUs with a global batch size of 1,024 (256 per GPU). We optimized parameters using AdamW with a cosine annealing learning rate schedule, spanning a total of 100 GPU hours. Mixed-precision training (FP16) was employed to enhance computational efficiency while maintaining stability. We use the learning rate of 5e - 5. We use hyperparameter λ as 0.01 to keep the same number scale as the divergence.

Kernel density estimator. A proper kernel size is critical in KDE for accurate estimation of Eq. (8). In this paper, we follow (Yin et al., 2024) to normalize the features from two modalities and use a kernel size 1. In general, this is sufficient to ensure stable learning.

C.1. T2I details

Kandinsky details. We use Kandinsky v2.2, an unCLIP-type model that utilizes CLIP ViT-bigG-14-laion2B-39B-b160k with 1280 projection dimensions for text and image encoders. Kandinsky v2.2 employs a latent diffusion model and MOVQ (Zheng et al., 2022) as the decoder to generate images of size 512×512 from the given image representation. When using the Kandinsky decoder, we apply 50 denoising steps (Ho et al., 2020) with a classifier-free guidance scale of 7.5 (Ho & Salimans, 2022).

Karlo details. Karlo uses CLIP-ViT-L/14 with 768 projection dimensions for image and text encoders. It employs a diffusion model to decode the image representation into a low-resolution image, followed by a super-resolution diffusion module that upsamples it to 512×512 . When using the Karlo decoder, we apply 25 denoising steps with a classifier-free guidance scale of 7.5, followed by an additional 7 super-resolution steps.

Adapter details. To ensure a fair comparison, our adapter module has the same architecture as Eclipse (Patel et al., 2024), which is based on the standard PriorTransformer model (Ramesh et al., 2022) but modified to be time-independent. Specifically, it consists of 10 layers with 16 attention heads, each having a head dimension of 32. The embedding dimension is 768/1280, with three additional embeddings. The model does not use time embeddings and has a dropout rate of 0.0.

LoRA We configure LoRA (Low-Rank Adaptation) for CLIP with a rank of r=8 and a scaling factor of $\alpha=16$, enabling efficient adaptation while maintaining a low computational footprint. The targeted modules include the self-attention projections, the fully connected layers, and the text_projection layer, ensuring adaptation across both vision and text processing components. A dropout rate of 0.1 is applied to enhance regularization. For the CLIP encoder in Kandinsky, ViT-bigG-14-laion2B-39B-b160k, the number of LoRA parameters is 6 million. As for CLIP-ViT-L/14 in Karlo, the CLIP model size is smaller, resulting in 1.3 million LoRA parameters.

LAION-HighResolution-5M selection. We use a subset of 5 million image-text pairs from the LAION-HighResolution dataset, which contains 175 million pairs. Due to computational constraints, we download only a portion of the dataset and select pairs with English captions.

D. More experimental results

Alignment with InfoNCE is not enough for the generation task. We train the adapter solely with InfoNCE and use the Kandinsky decoder to generate the corresponding images. Table 5 shows that InfoNCE alone struggles to align the multimodal distributions, resulting in a high FID score.

Table 5: **Ablation study of CS-Aligner.** Alignment with CS-Aligner significantly outperforms the alignment results with only InfoNCE.

Loss	FID
InfoNCE	151.35
CS-Aligner	12.62

D.1. More visualization

We illustrate more high-resolution images generated by the Kandinsky decoder with our aligned text representation in Fig. 7. The adapter is trained on LAION-HighRes 5M.

D.2. More visualization for token alignment

We provide more visualizations with and without the token alignment Fig. 8, demonstrating its ability to generate more fine-grained images with CS-Aligner.

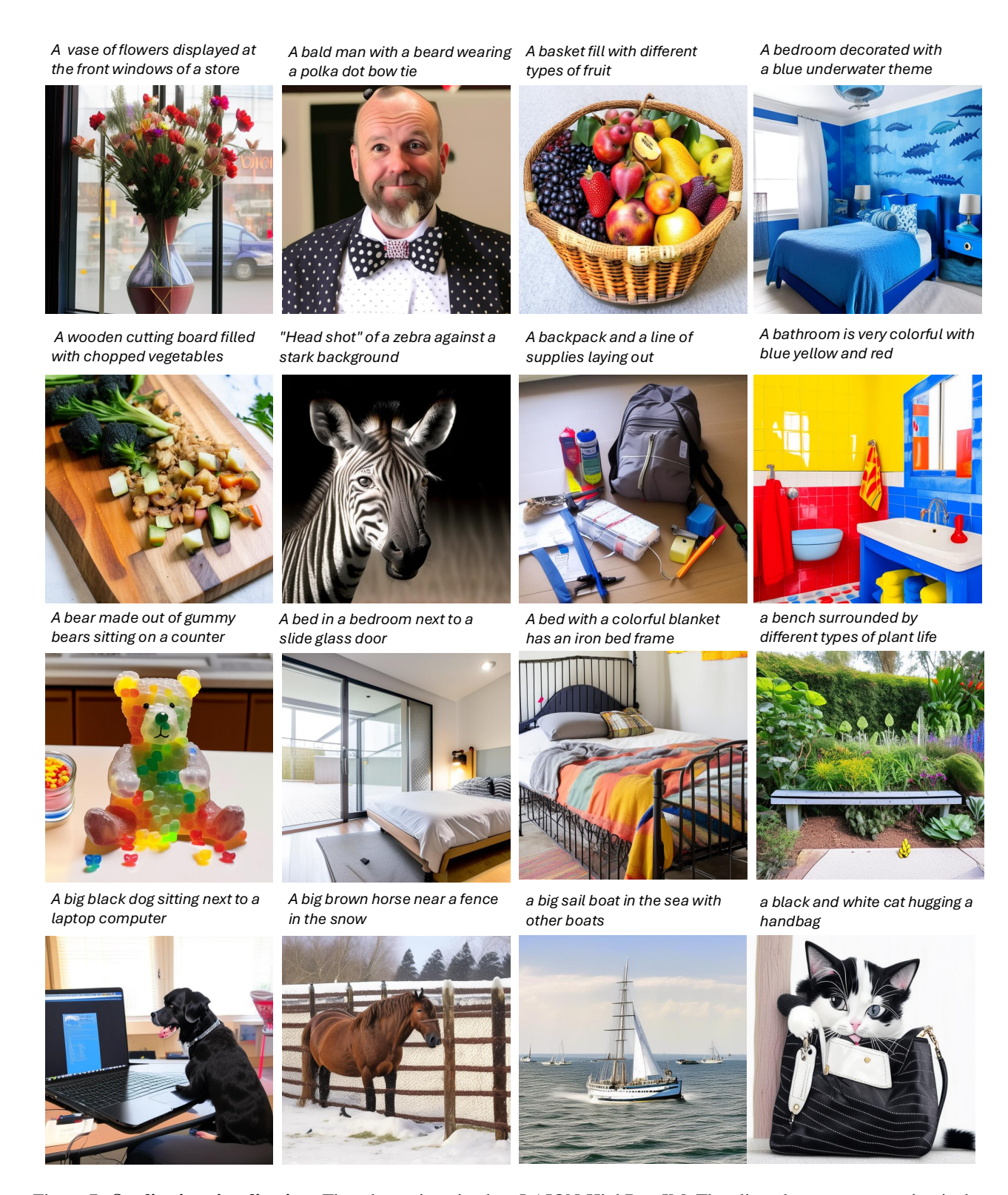


Figure 7: **Qualitative visualization.** The adapter is trained on LAION-HighRes 5M. The aligned text representation is then decoded by the Kandinsky decoder.



Figure 8: Token alignment is effective for fine-grained generations with more details and stronger semantic correspondence with the text inputs.